JOURNAL OF PROPULSION AND POWER
Vol. 25, No. 3, May–June 2009

Experimental and Numerical Study of Jet Mixing from a Shock-Containing Nozzle

Qing Xiao*
University of Strathclyde, Glasgow, Scotland G4 0LZ, United Kingdom
Her Mann Tsai†
National University of Singapore, Singapore 119260, Republic of Singapore
and
Dimitri Papamoschou‡ and Andrew Johnson§
University of California, Irvine, Irvine, California 92697-3975

DOI: 10.2514/1.37022

The compressible jet plume emerging from a planar convergent–divergent nozzle containing a separation shock is investigated experimentally and numerically. The investigation encompasses exit-to-throat area ratios (A_e/A_t) from 1.0 to 1.8 and nozzle pressure ratios from 1.2 to 1.8. Experiments were conducted in a variable-geometry nozzle facility, and computations solved the Reynolds-averaged Navier–Stokes equations with several turbulence models. The computed mean velocity field outside the nozzle compares reasonably well with the experimental data. Among the different turbulence models tested, the two-equation shear stress transport model is found to provide the best agreement with the experiments. Jet mixing is governed by A_e/A_t and, to a lesser extent, by nozzle pressure ratios. Increasing A_e/A_t results in an increased growth rate and faster axial decay of the peak velocity. The experimental trends of jet mixing versus A_e/A_t and nozzle pressure ratios are captured well by the computations. Computations of turbulent kinetic energy show that, with increasing A_e/A_t, the peak turbulent kinetic energy in the plume rises and moves toward the nozzle exit. The significant increase of turbulent kinetic energy inside the nozzle is associated with asymmetric flow separation.

Nomenclature

A	=	nozzle area
d	=	jet thickness
H	=	nozzle height
J	=	momentum flux
M	=	Mach number
m	=	mass flux of jet plume
p	=	mean pressure
T	=	mean temperature
U_{pe}	=	perfectly expanded velocity
u	=	mean axial velocity
x	=	axial coordinate
y	=	transverse coordinate

Subscripts

0	=	total
a	=	ambient
e	=	nozzle exit
max	=	peak value at fixed x
res	=	reservoir
t	=	throat location

Presented as Paper 1319 at the 45th AIAA Aerospace Sciences Meeting and Exhibit, Reno, NV, 8 January 2007–11 January 2008; received 5 February 2008; revision received 26 November 2008; accepted for publication 26 November 2008.

*Lecturer, Department of Naval Architecture and Marine Engineering.
†Principal Research Scientist, Temasek Laboratories. Member AIAA.
‡Professor, Department of Mechanical and Aerospace Engineering. Associate Fellow AIAA.
§Graduate Student Researcher, Department of Mechanical and Aerospace Engineering. Student Member AIAA.

I. Introduction

SUPERSONIC flow separation in a convergent–divergent nozzle results in the instability of the plume exiting the nozzle. This can be used to enhance mixing of the nozzle flow itself and/or of another flow adjacent to the nozzle. Potential applications include fuel injection, ejectors, and thermal signature reduction from jet engines. The instability phenomenon was initially observed in coannular jet experiments at the University of California, Irvine [1], in which an arbitrary primary jet surrounded by a secondary jet from a convergent–divergent nozzle showed substantial improvements in mixing compared with the case in which the secondary nozzle was simply convergent. Figure 1 presents a visual example of such instability. A typical result in round and rectangular jets is that the length of the potential core is reduced by 50% and the velocity past the potential core decays at a much faster rate than for the equivalent jet without the instability [1]. For a nozzle with a given expansion ratio, the range of nozzle pressure ratios over which the instability occurs coincides with the range of nozzle pressure ratios for which a shock is located inside the nozzle. Therefore, the phenomenon of supersonic nozzle flow separation was deemed responsible for the observed instability. The critical parameters of this problem include the exit-to-throat area ratio, A_e/A_t, and the nozzle pressure ratio (NPR), p_{res}/p_a. Other variables, such as wall exit angle, may also play a role but are not systematically addressed in this study.

Several past studies have investigated supersonic nozzle flow separation [2–10], but their focus was on the internal flow phenomena and not so much on the unstable plume that emerges from the separation shock. To better understand supersonic nozzle flow separation and its connection to the observed flow instability, a specialized planar nozzle with variable wall geometry was built and will be described later in this paper. Initial experiments in a symmetric nozzle [7] showed that separation becomes asymmetric for $A_e/A_t \geq 1.4$ and NPR > 1.4. Figure 2 shows a spark schlieren image and a sketch of the basic features of the flowfield. The shock in the viscous case takes on a bifurcated structure consisting of an incident shock and a reflected shock merging into a Mach stem. This is commonly referred to as a lambda foot, and the point at which the three components meet is called the triple point. For the range of

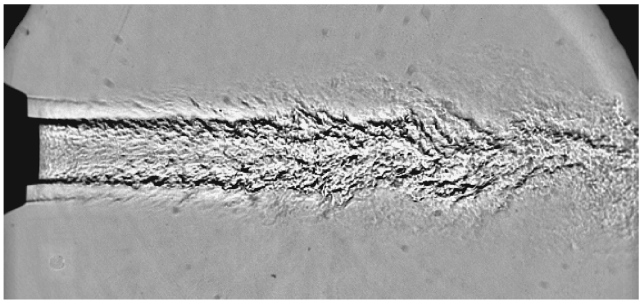

a)

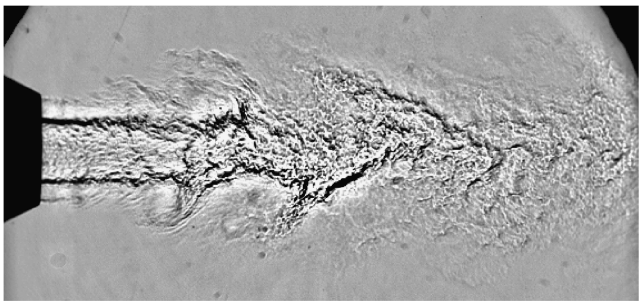

b)

Fig. 1 Primary jet flow at Mach 0.9 surrounded by an annual secondary flow at a nozzle pressure ratio of 1.7: a) secondary nozzle is convergent, and b) secondary nozzle is convergent–divergent.

conditions of interest here, the incident and reflected shocks are of the "weak" type resulting in supersonic outflow past both. The adverse pressure gradient of the incident shock causes the boundary layer to separate and detach from the wall as a shear layer that bounds the separation (recirculation) region. Emerging from the triple point is a slipstream forming a sonic throat that acts to reaccelerate the subsonic region. The reflected portion of the main shock structure will then emerge from the separation shear layer as an expansion fan. That expansion fan is then transmitted through the slipstream toward the other separation shear layer, where it is reflected again into compression waves, this pattern repeating with downstream

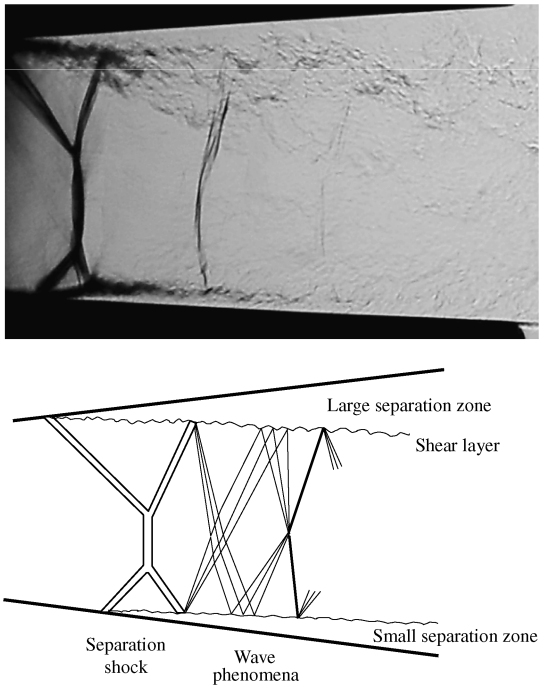

Fig. 2 Picture and sketch of principal flow features of supersonic nozzle flow separation [4].

distance. Therefore the separation "jet" that emerges from the shock contains a series of alternating compression and expansion waves.

In nozzles with straight or convex walls subjected to nozzle pressure ratios above about 1.4, separation is asymmetric wherein one lambda foot is larger than the other (see Fig. 2). The asymmetry does not flip during an experiment but may change sides from one experiment to the next. A recent computational effort by Xiao et al. [8] also demonstrated this asymmetric shock and separation inside the nozzle. This asymmetry has been recognized as a key factor for mixing enhancement. Papamoschou and Zill [7] discovered large eddies forming in the shear layer of the large separation region, sometimes occupying over half the test section height. It was suspected that these eddies were due to the unsteady nature of the main shock.

The current work expands on the nozzle studies of Papamoschou and Zill [7] and Xiao et al [8] to include the turbulent jet region downstream of the nozzle exit. The purpose of our investigation is twofold: 1) assess experimentally the effects of nozzle parameters (area ratio, pressure ratio) on the mean flow characteristics of the jet plume, and 2) evaluate the ability of computations to capture the experimental trends. If the numerical approach is successful, it could be used for optimizing mixing-enhancement configurations as well as providing information that is difficult to measure experimentally. The computations build on past successful efforts to compute the internal nozzle flow, such as the works by Hunter [5], Xiao et al. [8,10], and Carlson [9].

However, it is noted that reliable and accurate computations of the turbulent jet plume are not without their challenges, particularly where the Reynolds-averaged Navier–Stokes (RANS) method is concern. Its accuracy not only depends on the numerical method but also critically on the modeling of the turbulence. The effect of different turbulence models on the prediction of jet mixing has been investigated by several works. In the prediction of compressible jet plumes, it was found essential to include a compressibility correction to the standard k–ε model; such a correction was first proposed by Sarkar et al. [11] and also demonstrated by Zeman [12], Huang et al. [13], Thies and Tam [14], and Tandra et al. [15]. Chenault and Beran [16] conducted a numerical investigation of supersonic injection using second-order Reynolds-Stress turbulence model proposed by Zhang et al. [17] as well as the k–ε model. Detailed comparisons with experimental data showed that the Reynolds-stress model simulation results in physically consistent and accurate prediction for jet plume mean flow and turbulent quantities. However, the simulations with the k–ε model resulted in nonphysical and inconsistent turbulence prediction. Dembowski and Georgiadis [18] conducted a numerical study for supersonic axisymmetric jet flow using the two-equation shear stress transport (SST) and k–ε models, with and without compressibility correction. Their results indicated that the compressibility correction significantly improves the solution. Georgiadis and Papamoschou [19] investigated single and coaxial dual-stream jets using RANS with linear two-equation and nonlinear two-equation explicit algebraic stress turbulence modeling. Their comparison of computed mean flowfield development with experiments shows that the standard SST model provides the overall best agreement with experimental data.

The present study does not attempt to make a critical assessment of turbulence models with the data obtained, as only wall-pressure and pitot measurements are used as primary diagnostics and no turbulence measurements were made. Instead, as will be apparent, recognizing the limitations of the RANS-type models, the approach is a practical one in which we use a model that appears to offer overall agreement with the experimental data collected. The interest is to examine to what extent numerical computations with the RANS model offer us the trends observed in the experiment. It is hoped that such computations are sufficiently accurate to assess the fluidic phenomenon for jet mixing studies.

The rest of the paper is organized in the following manner. The facilities used and the computational method adopted are briefly outlined. This is followed by a discussion of the experimental and numerical results and concluding remarks.

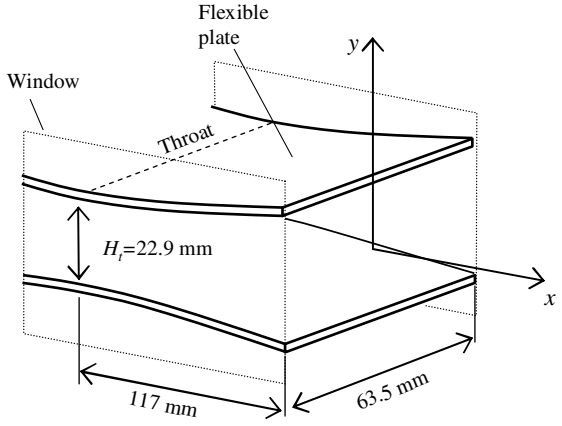

Fig. 3 Schematic of nozzle apparatus.

II. Experimental Details

The experiments used a facility designed specifically for studying flow separation in nozzles of various shapes, detailed in [7]. The salient features relevant to this study are shown in Fig. 3. The nozzle is rectangular with an aspect ratio at the throat of 2.8. The upper and lower nozzle walls are formed by flexible plates that can be shaped using actuators attached to their ends. One set of actuators controls the transverse force and the other set controls the moment applied to the end of each plate. This allows variations in nozzle area ratio, nozzle contour, and exit angle. In this study, only the former set of actuators was used, resulting in a "trumpet-shaped," symmetric nozzle. The nominal test section dimensions are 22.9 mm in height, 63.5 mm in width, and 117 mm in length from throat to exit. The sidewalls of the nozzle incorporate large optical windows for visualization of the entire internal flow, from the subsonic converging section to the nozzle exit. The apparatus is connected to a system of pressure-regulated air capable of nozzle pressure ratios as high as 3.5.

Each nozzle wall is fitted with 24 equally spaced pressure ports extending from an area ratio of $A/A_t = 1.14$ upstream of the nozzle throat to the nozzle exit. The 0.8-mm-diam ports were scanned by a mechanical pressure multiplexer (Scanivalve model SSS-48), which consists of a pneumatic selector switch connected to a single pressure transducer (Setra model 280). This measurement gives the time-averaged wall pressure distribution over the entire nozzle. It was shown in previous studies that the pressure recovery on the wall with a large separation zone has a distinctive linear rise, whereas on the wall with a small separation zone the pressure shows a faster initial rise followed by a gradual recovery to the ambient value [1]. This trend has also been observed in computations of nozzle flow separation [3] and allows differentiation between the walls with small and large separation zones.

In the present study, the NPR ranged from 1.2 to 1.8, resulting in perfectly expanded velocities, U_{pe}, ranging from 170 to 320 m/s. The Reynolds number before the shock, based on the axial distance from the throat, was on the order of 2.5×10^6, which corresponds to a fully turbulent boundary layer. Mean velocity measurements in the jet plume were obtained by means of a pitot probe with a piezoresistive transducer (Endevco model 8507C) at its tip. This arrangement allows for time-resolved measurement of the total pressure, although this paper covers only the time-averaged values. The velocity was calculated from the total pressure assuming $p = p_a$ and $T_0 = T_a$ in the nozzle plume. All the measurements presented are on the vertical center plane of the nozzle (x–y plane shown in Fig. 3).

III. Computational Method

The RANS equations were solved using the commercial code FLUENT. Inviscid fluxes were calculated using a second-order upwind scheme, whereas the viscous fluxes were evaluated using a second-order central-difference scheme. A second-order implicit scheme was used for iterating the unsteady equations to the steady-state solution. The computations were made using two-dimensional assumptions. As a cautionary note, Hunter [5] reported that significant differences exist between 2-D computational results and the experimental data for nozzles for which the NPR values are less than 2.4. He pointed out that the differences were due to the fact that the flow became very three dimensional at the low NPR values. Xiao et al. [10] also observed similar behavior in their two-dimensional computations of Hunter's experiment. However, for the nozzle under investigation here, our schlieren pictures of the flow in the nozzle appear remarkably two dimensional for the area ratio and NPR under investigation. In our previous paper describing a flow of similar geometry [8], the computed wall pressure distribution using a 2-D assumption also shows good agreement over a range of exit-to-throat area ratios (A_e/A_t) from 1.0 to 1.8 and NPR from 1.2 to 1.8, which are also used for our present study. As such, the computed results reported here are all obtained from two-dimensional computations.

The wall boundary layer was assumed to be turbulent, and the two-equation SST model of Menter [20] is used here. The SST model employs a k–ω formulation in the inner region of wall boundary layers and switches to a transformed k–ε formulation in the outer region of boundary layers and in the free shear layer. The compressibility correction of Sakar et al. [11] is adapted.

The computational flow conditions matched the experimental conditions, that is, A_e/A_t ranged from 1.0 to 1.8 and NPR ranged from 1.2 to 1.8. For each area ratio, the computational nozzle matched exactly the geometry of the experimental nozzle.

The computational domain included the domain inside the nozzle and an ambient region around the outer surface and downstream of the nozzle with 25 throat heights downstream, 15 upstream, and 10 normal to the jet axis. The computation was performed on a structured grid generated by a separate, in-house code, as illustrated in Fig. 4. For clarity, Fig. 4 displays only every forth grid line in each direction. There were a total of about 74,000 cells distributed among the aforementioned regions. Grid points were clustered near the walls of the nozzle to resolve the boundary layers and at the exit of the nozzle to resolve the recirculation zone. For a Reynolds number based on the throat height of 2.5×10^6, the minimum first grid point from the wall gives $y^+ < 1$. Three sets of grid cells, a coarse grid of about 18,000, a medium grid of about 74,000, and a fine grid of 240,000, were used for the grid-dependence study. The predicted axial decay for the peak velocity in the jet plume is shown in Fig. 5 together with the experimental data. The results indicate that 74,000 cells are adequate for capturing the main flow characteristics in the jet plume.

The boundary conditions were imposed as follows: the total pressure and total temperature at the inlet were set to be $p_{\text{res}} = \text{NPR} \times p_a$ and $T_{\text{res}} = T_a$, respectively, where $p_a = 14.85$ psi and $T_a = 294$ K. The walls were specified to be adiabatic with a no-slip condition. The downstream static pressure was set to the ambient pressure.

The computation was conducted with the FLUENT unsteady RANS code. However, the computed shock location inside the nozzle and the pressure monitored at points $(x - x_t)/H_t = 1.0$ and $y/H_t = 0.5$ show the flow to assume a steady state in contrast to the experiment, in which the flow is observed to show random unsteadiness. This difference is not entirely clear but is consistent with our earlier computation of internal nozzle flow [8] using an in-house unsteady RANS code.

The Courant–Friedrichs–Lewy number used ranged from 0.5 to 5 over a few thousand iterations. Convergence of the momentum equation typically required about 7000 iterations to reduce the L2 norm of the residual by 2–3 orders of magnitude.

IV. Results and Discussion

Experiments were conducted to study the effects of exit-to-throat area ratios and nozzle pressure ratios using the variable-geometry nozzle facility. Corresponding computations were performed to examine the extent to which the computation captures the internal flow phenomena and external mean flow trends of the experiments. As noted earlier, the intent is to establish the computational method

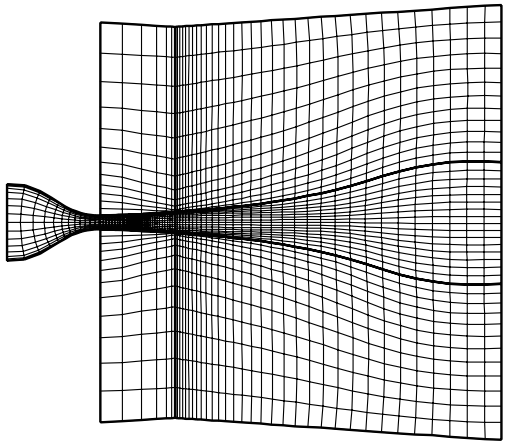

a)

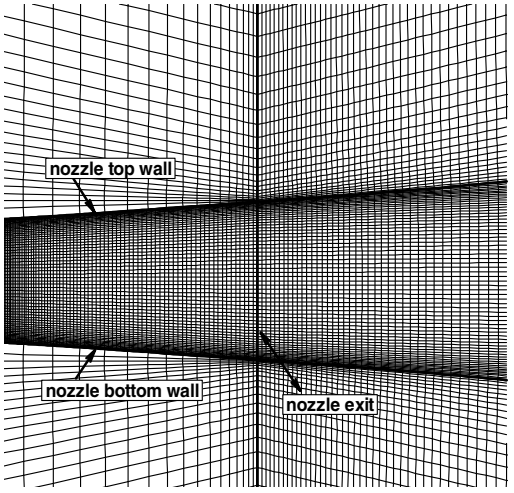

b)

Fig. 4 Computational domain and mesh: a) overall view (only every 4th grid point is displayed), and b) close-up view near nozzle exit (every grid point indicated).

as a means to examine the influence of area and pressure ratio on the instability of the jet plume arising from an overexpanded, shock-containing convergent–divergent nozzle.

A. Flow Pattern in the Nozzle

The typical computed Mach number contours inside and outside the nozzle for $A_e/A_t = 1.5$ and NPR $= 1.6$ are shown in Fig. 6. The

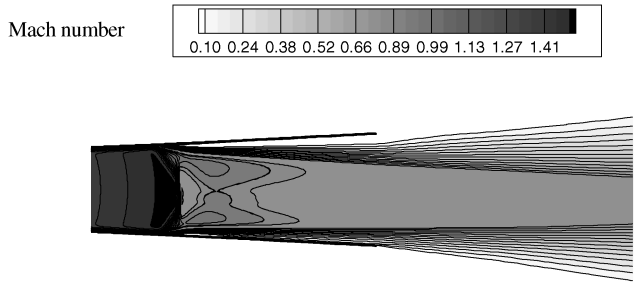

Fig. 6 Mach number contours inside and outside the nozzle for $A_e/A_t = 1.5$ and NPR $= 1.6$.

basic flow features are in agreement with the experimental results of Fig. 2. It is seen that a well-defined lambda shock appears inside the nozzle. In agreement with observations of past experimental work [7] and earlier computations [8], an asymmetric flow pattern is observed with a large lambda foot occurrence at one wall and a small foot at the opposite wall for this NPR value. In the sections that follow, we discuss the basic mixing trends with A_e/A_t and NPR.

Before conducting a detailed computation, test cases were run using different turbulence models for $A_e/A_t = 1.5$ at NPR $= 1.6$, and the results were compared with the experimental data. The turbulence models comprised a one-equation Spalart–Allmaras (SA) model [21], a two-equation realizable k–ε model [22], Wilcox's standard k–ω model [23], the SST model of Menter [20], and the Reynolds-stress model [24] (RSM). It should be emphasized that the

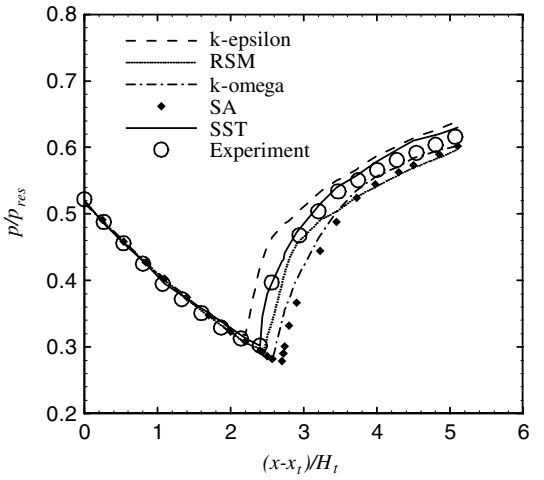

Fig. 7 Wall static pressure distribution on the large separation for $A_e/A_t = 1.5$ and NPR $= 1.6$.

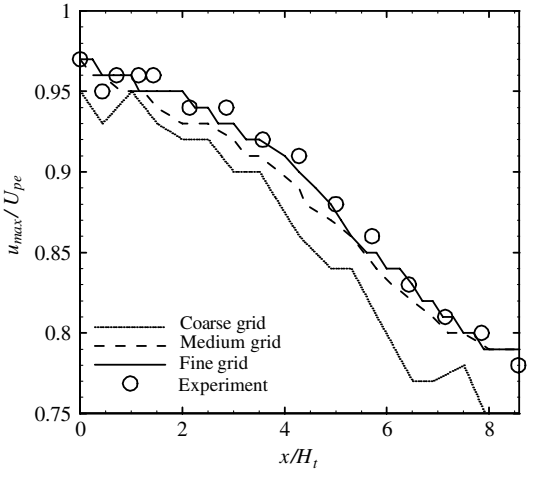

Fig. 5 Grid dependence of peak velocity distribution in the jet plume.

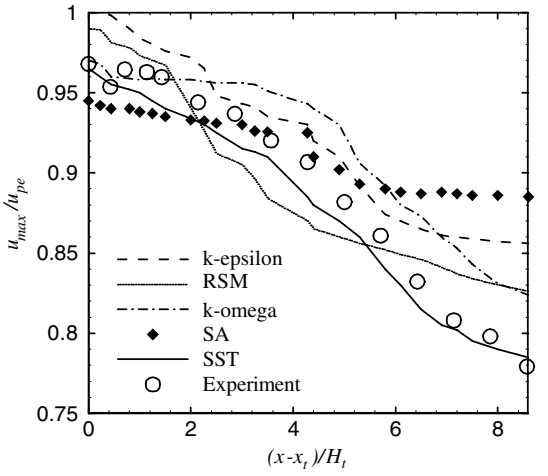

Fig. 8 Distribution of peak velocity in the jet plume.

intention here is not so much as to make a detailed assessment of the different models and their various variants in computing the present flow. Rather it is to select among these models one that can represent flow.

Figure 7 shows the wall pressure distribution on the large separation side for the five different turbulence models as well as the experiment. All five models show excellent agreement with the experiment upstream of the shock. The shock location is overpredicted (downstream of the experimental value) by the RSM, k–ω, and SA models, whereas it is underpredicted by the k–ε model. Among the five turbulence models, the SST model best captures the shock location and pressure distribution of the experiment. We believe that the superior performance of the SST model is brought about by the correct prediction of flow separation just downstream of the shock caused by shock–boundary-layer interaction inside the nozzle.

B. Flow in the Jet Region

A common measure of jet mixing is the axial decay of the peak mean velocity, $u_{\max}$. Figure 8 plots $u_{\max}(x)/U_{\text{pe}}$ for the five different turbulence models and for the experiment. It is again evident that the SST model produces the best agreement with the experimental data,

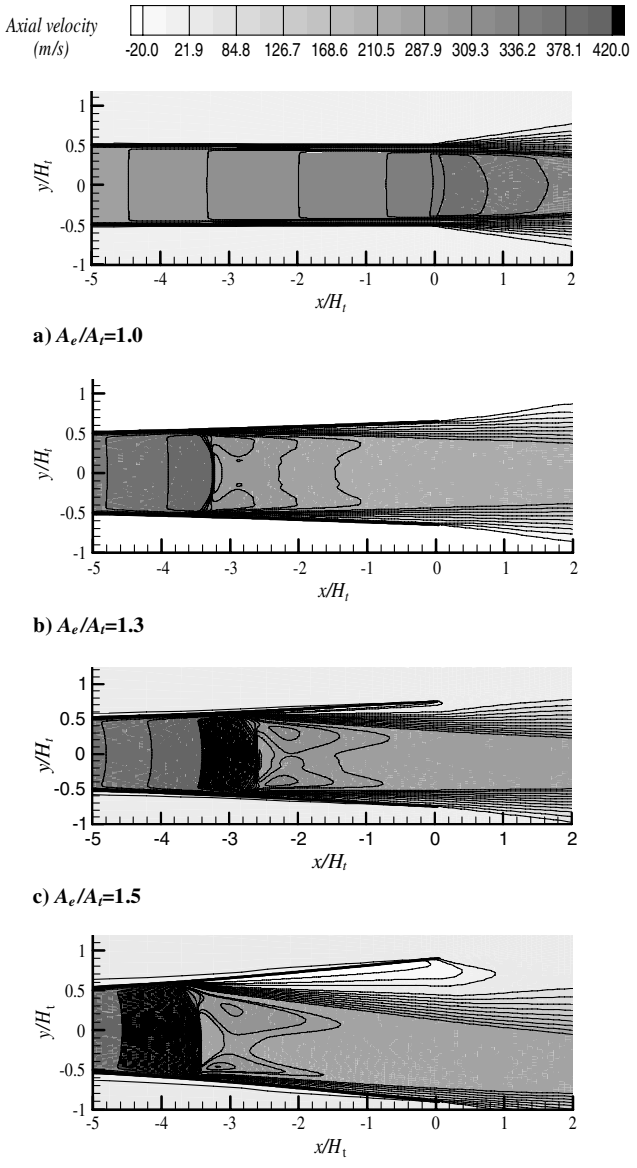

a) A_e/A_t=1.0

b) A_e/A_t=1.3

c) A_e/A_t=1.5

d) A_e/A_t=1.8

Fig. 9 Effect of area ratio on the mean axial velocity distribution for NPR = 1.6.

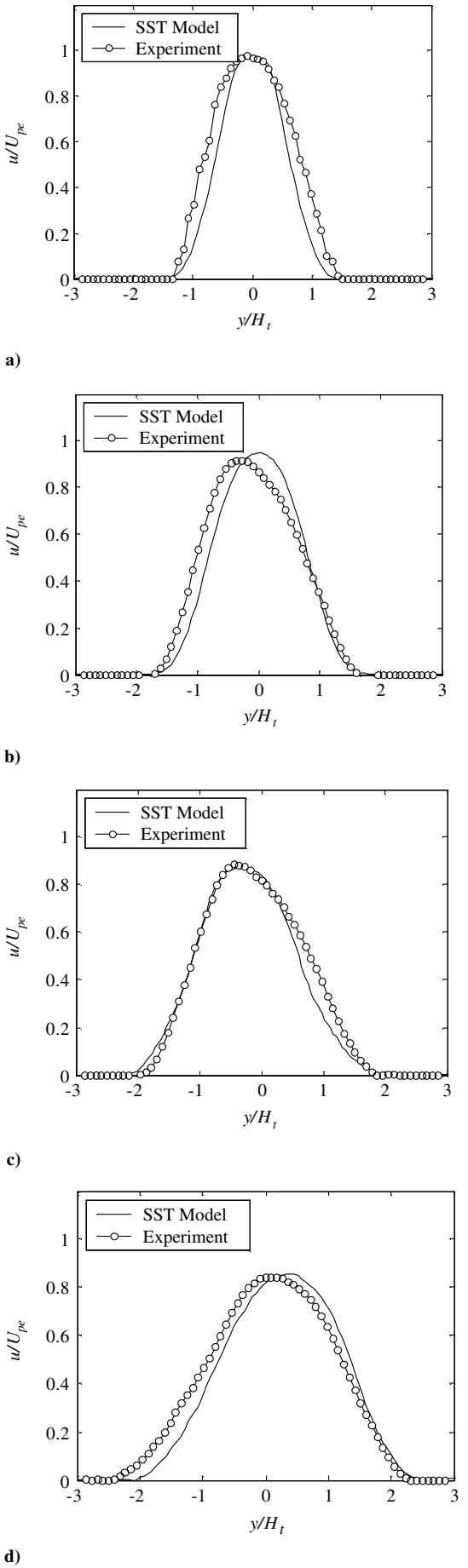

a)

b)

c)

d)

Fig. 10 Velocity profiles at $x/H_t = 4.6$: a) $A_e/A_t = 1.0$, b) $A_e/A_t = 1.3$, c) $A_e/A_t = 1.5$, and d) $A_e/A_t = 1.8$.

consistent with its superiority in predicting the wall pressure distribution. For this reason, the SST model is used for the computations in the remainder of this paper.

In the following section, we evaluate the mixing of the jet plume in terms of the basic parameters of the problem: the area ratio A_e/A_t and the NPR. As it will be shown, the NPR plays a relatively minor role in jet mixing provided its range is consistent with the occurrence of supersonic nozzle flow separation. Therefore, our discussion will emphasize the effect of area ratio.

The evolution of the flowfield at a fixed NPR of 1.6 and variable A_e/A_t is captured in the velocity isocontour plots of Fig. 9. As the area ratio increases, the separation shock becomes asymmetric. On the large separation side, a thick shear layer develops and forms a thickened jet outside the nozzle. The evolution of the plume velocity profile at a fixed axial location with A_e/A_t is depicted in Fig. 10. The broadening of the profile and its departure from symmetry are evident as A_e/A_t increases from 1.0 to 1.8. The computation captures this trend very well, except that it predicts a slightly narrower profile for $A_e/A_t = 1.0$.

C. Jet Mixing Trends

Figure 11 shows the experimental measurements and computational prediction of the axial distribution of the peak velocity, $u_{\max}(x)/U_{\text{pe}}$, for NPR $= 1.6$ and a variable A_e/A_t. For $A_e/A_t = 1.0$, we observe a flat distribution until about $x/H_t = 4$, indicating the extent of the potential core. As A_e/A_t increases, $u_{\max}$ starts decaying immediately past the nozzle exit, suggesting the disappearance of the potential core. The decay rate becomes more pronounced with increasing A_e/A_t, indicating faster mixing of the jet plume with the ambient air. The computations capture the experimental trends very well. The effect of NPR on the decay of $u_{\max}$ for $A_e/A_t = 1.5$ is shown in Fig. 12. For NPR $= 1.2$, the velocity decays relatively slowly, indicating no significant mixing enhancement. For NPR $= 1.4$–1.6, the decay becomes much more pronounced, indicating vigorous mixing. With NPR increasing to 1.8, we observe a slight reduction of the decay, which is still much faster than the decay for NPR $= 1.2$. Therefore, for $A_e/A_t = 1.5$, and for this particular nozzle shape, the best mixing enhancement occurs for $1.4 \leq \text{NPR} \leq 1.6$. It is noteworthy that the computations capture this trend qualitatively and quantitatively.

Figures 13 and 14 show the axial growth of the plume thickness for a variable A_e/A_t (with a fixed NPR) and a variable NPR (with a fixed A_e/A_t), respectively. It is seen that the area ratio has a major impact on jet thickness, with δ at a fixed axial location roughly doubling as A_e/A_t increases from 1.0 to 1.8. On the other hand, the NPR has a smaller impact, with the fastest growth occurring for $1.4 \leq \text{NPR} \leq 1.6$, consistent with the velocity decay results of Fig. 12. We note once again the very good comparison between the experimental results and computational predictions. The plume growth rate is obtained by a linear least-squares fit through the axial thickness distribution. The experimental and computational growth rates for NPR $= 1.6$ are plotted versus A_e/A_t in Fig. 15. The growth

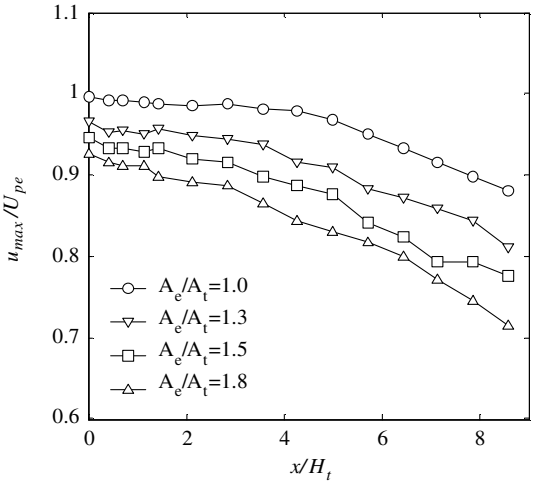

a) Experiment

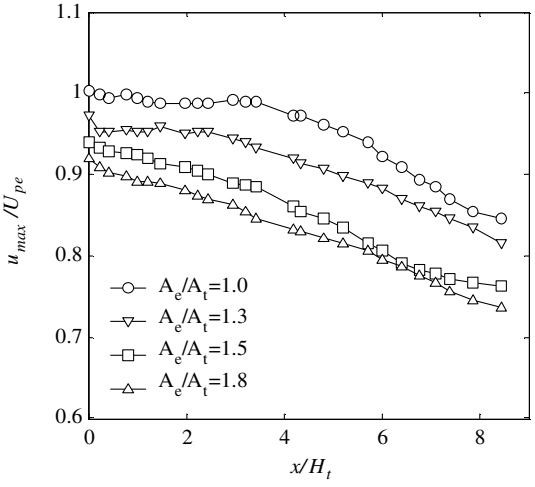

b) Computation

Fig. 11 Effect of nozzle area ratio on axial distribution of peak velocity for NPR = 1.6.

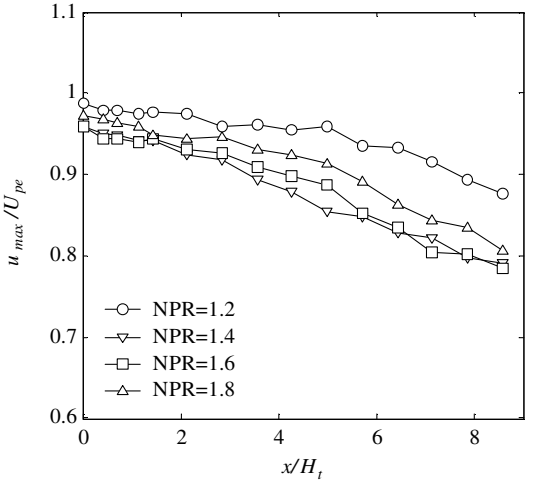

a) Experiment

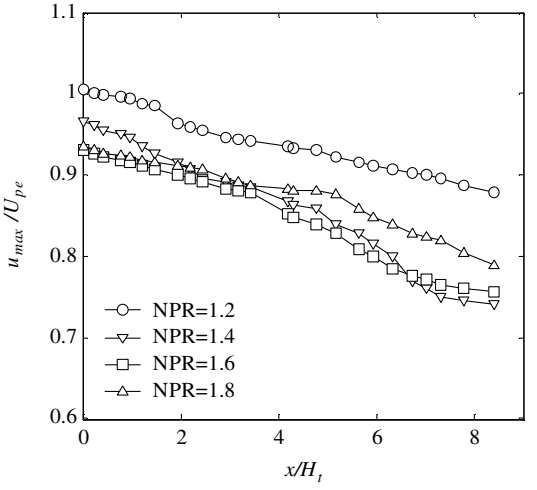

b) Computation

Fig. 12 Effect of nozzle pressure ratio on axial distribution of peak velocity for $A_e/A_t = 1.5$.

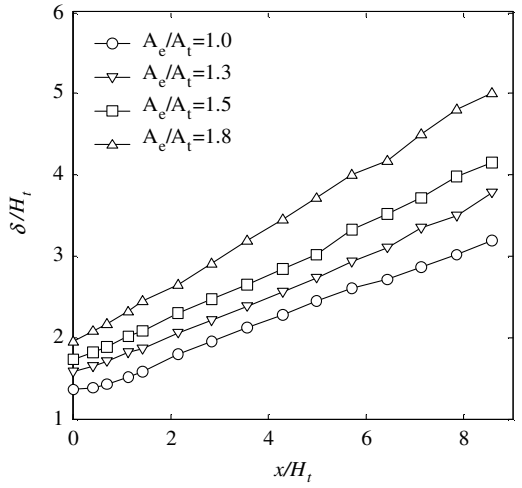

a) Experiment

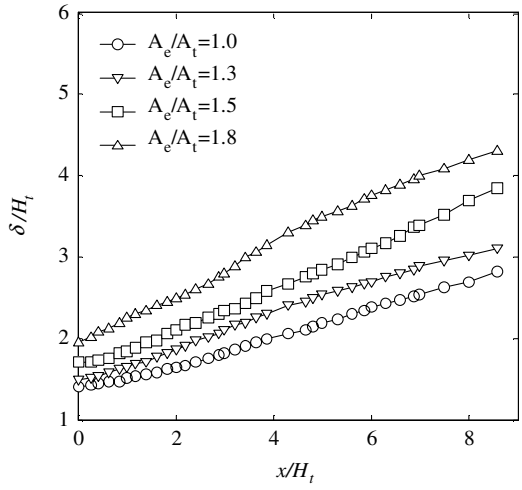

b) Computation

Fig. 13 Effect of nozzle area ratio on axial distribution of jet thickness for NPR = 1.6.

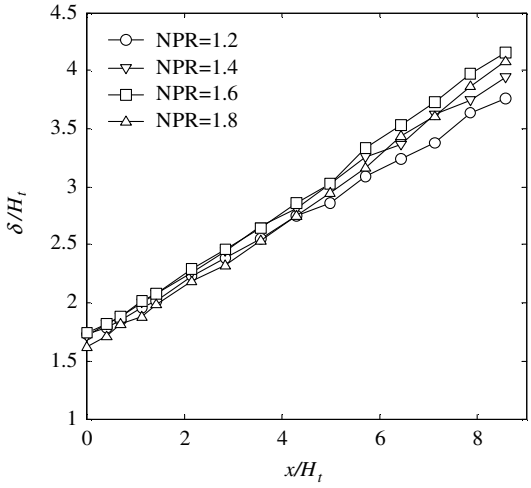

a) Experiment

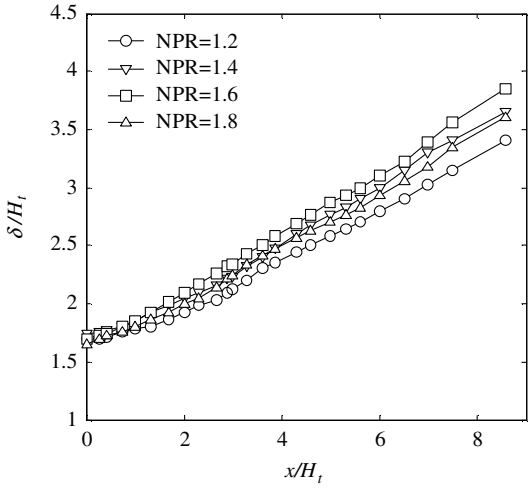

b) Computation

Fig. 14 Effect of nozzle pressure ratio on axial distribution of jet thickness for $A_e/A_t = 1$.

rate increases by about 70% as A_e/A_t increases from 1.0 to 1.8. The computations generally agree well with the experiment except that they slightly underpredict the growth rate at NPR = 1.8.

The general agreement between the computation and the experiment provides us with confidence that the computation can provide accurate predictions of quantities not easily measured in the experiment. Here we consider the jet mass flow rate and the turbulent kinetic energy distribution inside and outside the nozzle. In the experiment, the mass flow rate is difficult to measure because the integration needs to extend to the edges of the jet where the velocity is poorly resolved. The measurement of turbulent fluctuation velocities in a high-speed environment is an even bigger challenge due to the limitations of diagnostic techniques, such as hot wires and particle image velocimetry.

An additional measure of jet mixing, or entrainment, is the mass flow rate of the jet plume. In our case, we define it in a two-dimensional sense as

$$m(x) = \int_{y_{\text{lower}}(x)}^{y_{\text{upper}}(x)} \rho u \, \mathrm{d}y$$

where $y_{\text{upper}}(x)$ and $y_{\text{lower}}(x)$ represent the upper and lower edges of the jet, respectively. Each edge is at the region where the velocity drops to around 1% of its peak value at each axial location and is adjusted such that the momentum flux

$$J = \int_{y_{\text{lower}}(x)}^{y_{\text{upper}}(x)} \rho u^2 \, \mathrm{d}y$$

is invariant with axial distance. The mass flow rate is computed from the velocity and density fields at each downstream location and is normalized by the nozzle exit value m_e to obtain the entrainment rate of the jet. Figure 16 shows the plots of m/m_e versus x/H_t for different nozzle area ratios. The entrainment for the baseline ($A_e/A_t = 1$) case starts very slowly and grows significantly past $x/H_t = 6$. As the area ratio increases, the region of growth moves toward the nozzle exit, and the growth itself becomes stronger. At $x/H_t = 6$, the entrainment for $A_e/A_t = 1.8$ is 60% stronger than for the baseline case.

D. Turbulent Kinetic Energy

The turbulent kinetic energy (TKE) is perhaps the most relevant quantity in terms of the ability of the flow emerging from the convergent–divergent nozzle to destabilize an adjacent flow, as shown in Fig. 1. Even though the present computation is not time accurate, the unsteadiness of the jet plume can be quantified in terms of the statistics of the velocity fluctuations. Here we consider the TKE defined as

$$k = \tfrac{1}{2}(\overline{u'^2} + \overline{v'^2} + \overline{w'^2})$$

where u', v', and w' denote the fluctuations of the three velocity components, and the overbars indicate time averaging. We note here

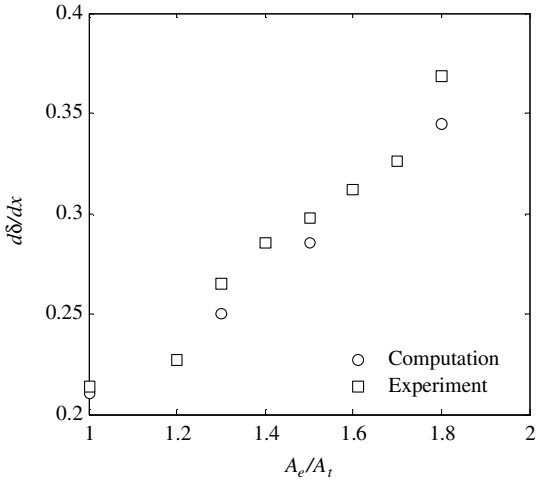

Fig. 15 Effect of nozzle area ratio on the jet growth rate for NPR = 1.6.

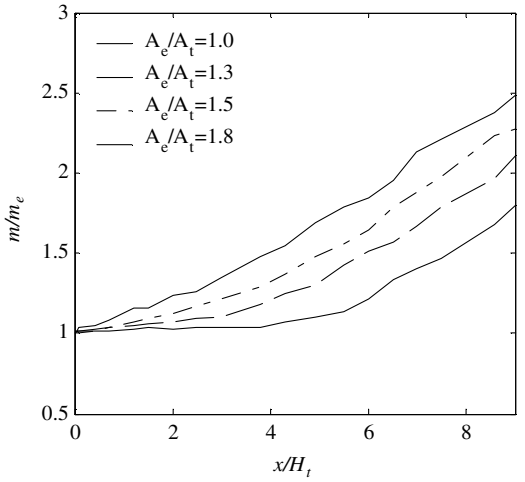

Fig. 16 Computational results for the effect of nozzle area ratio on entrainment for NPR = 1.6.

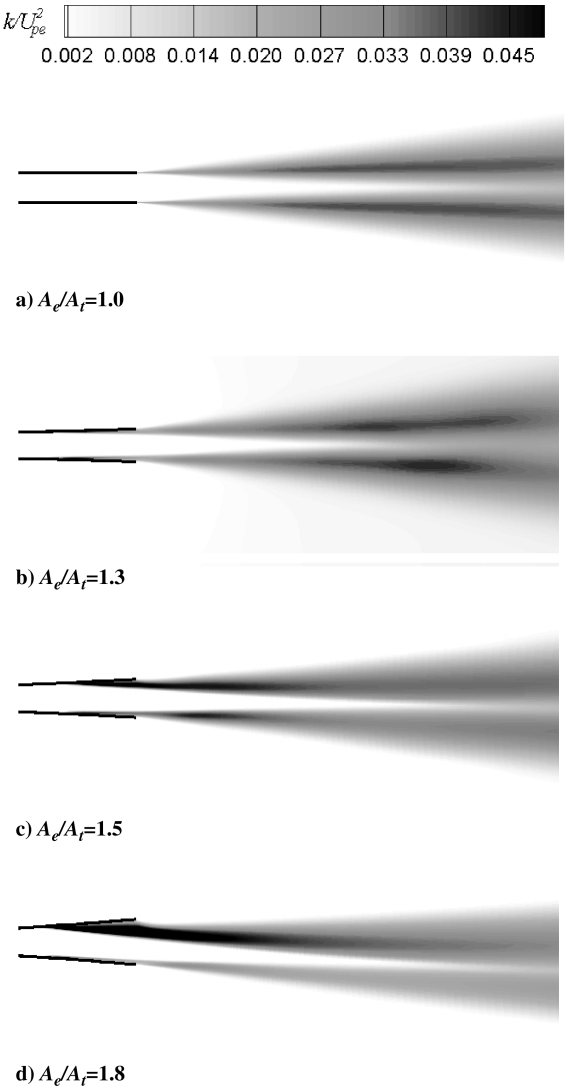

Fig. 17 Computational results for the effect of area ratio on the turbulent kinetic energy at NPR = 1.6.

that no experiments were made to measure the TKE. Figure 17 presents isocontours of the computed k/U_{pe}^2 for NPR = 1.6 and for different area ratios. For $A_e/A_t = 1.0$, the flow inside the nozzle is attached and the jet plume develops as in a normal jet. High levels of TKE are present in the shear layers, with the peak level occurring at $x/H_t = 5$, which is near the end of the potential core. As the area ratio increases, the peak TKE level moves closer to the nozzle. Simultaneously, we observe significant production of TKE inside the nozzle, as a result of the turbulent separated flow. The TKE levels in the far plume reduce as a consequence of the faster velocity decay caused by the mixing enhancement. For $A_e/A_t = 1.3$, the TKE distribution is symmetric, reflecting the symmetric shock formation inside the nozzle. For $A_e/A_t \geq 1.5$, the distribution becomes asymmetric due to the asymmetric shock formation. The TKE in the large separation zone is significantly larger than that in the small separation zone. As the nozzle area ratio increases from 1.0 to 1.8, the TKE near the nozzle exit rises by about threefold. Large turbulent intensities near the nozzle are a desirable feature for this flow to be used as a "fluidic actuator" in the sense captured by Fig. 1.

E. Nozzle Performance

As one of the proposed applications of the mixing enhancement is for aeroengines, it is important to assess the thrust loss caused by flow separation inside the nozzle. The thrust is estimated by the computed wall pressure distribution. The thrust coefficient is defined here as the ratio of the actual nozzle thrust to the perfectly expanded nozzle thrust. Figure 18 shows the thrust coefficient versus NPR for different nozzle area ratios. For $A_e/A_t = 1.3$, the thrust coefficient drops then rises with increasing NPR. For $A_e/A_t = 1.5$ and 1.8, the thrust coefficient rises monotonically with NPR. As expected, the thrust coefficient decreases with increasing area ratio due to the stronger shocks and higher total pressure loss. The system loss will depend on the relative contribution of this flow to the total thrust. Past

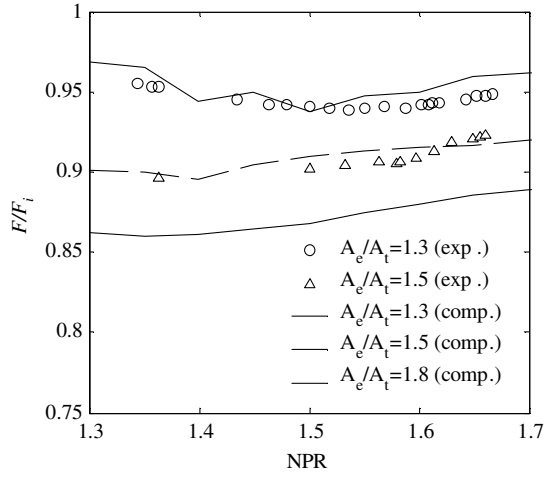

Fig. 18 Effects of NPR and area ratio on the thrust coefficient.

experiments have shown that as little as 10% of the unstable flow surrounding a jet can destabilize the jet [3]. In addition, one can explore on-demand implementations of this mixing-enhancement scheme.

V. Conclusions

We presented a joint experimental and computational study of the jet emerging from a convergent–divergent nozzle experiencing supersonic flow separation. The experiments were made in a variable-geometry nozzle rig, and the computations solved the Reynolds-averaged Navier–Stokes equations with the two-equation SST model. The investigation encompassed exit-to-throat area ratios (A_e/A_t) from 1.0 to 1.8 and NPR from 1.2 to 1.8.

For $A_e/A_t \geq 1.4$ and NPR > 1.4, flow separation is asymmetric resulting in a large separation zone on one wall and a small separation zone on the other wall in the nozzle before the jet is formed. Experimental data of the mean flow characteristics show the enhanced jet mixing to be governed by A_e/A_t and, to a lesser extent, NPR. For a fixed A_e/A_t, jet spreading increases then decreases with increasing NPR. Increasing A_e/A_t results in an increased growth rate and faster axial decay of the peak velocity. The basic flow structure of the separation, including its asymmetry, was captured qualitatively by the computation. Good agreement with the experimental data is obtained for the mean velocity profiles, the axial decay of the peak velocity, the thickness distribution in the jet plume, and the thrust coefficient. Computations of TKE show that, with increasing area ratio, the peak level of TKE in the plume rises and moves toward the nozzle exit. A significant increase of the TKE inside the nozzle is observed, a direct consequence of the asymmetric flow separation. A key result of this paper is that both the experiment and the computation indicate that the asymmetric separation plays significant role in the development of the jet plume. The computational approach used here appears to be a suitable tool for arriving at optimal nozzle shapes for mixing enhancement.

Acknowledgments

The authors at the National University of Singapore gratefully acknowledge the support from the Directorate of Research and Development, Defense Science and Technology Agency, Singapore under program managers K.Y. Lou (Flow Control Program) and A. Wong (Inlet & Nozzle Flow Program). The authors at the University of California, Irvine, gratefully acknowledge the support of contract TL/AE/2004/0001 from Temasek Laboratories, National University of Singapore, under program manager Her Mann Tsai. Paul Rossetti is thanked for his assistance with the experiments.

References

[1] Papamoschou, D., "Mixing Enhancement Using Axial Flow," AIAA Paper 2000-0093, Jan. 2000.

[2] Morrisette, E. L., and Goldberg, T. J., "Turbulent Flow Separation Criteria for Overexpanded Supersonic Nozzles," NASA TP 1207, Aug. 1978.

[3] Wilmoth, R. G., and Leavitt, L. D., "Navier–Stokes Predictions of Multifunction Nozzle Flows," Society of Automotive Engineers Paper 871753, Oct. 1987.

[4] Hamed, A., and Vogiatzis, C., "Overexpanded Two-Dimensional Convergent–Divergent Nozzle Flow Simulations, Assessment of Turbulence Models," *Journal of Propulsion and Power*, Vol. 13, No. 3, 1997, pp. 444–445. doi:10.2514/2.5183

[5] Hunter, C. A., "Experimental, Theoretical and Computational Investigation of Separated Nozzle Flows," AIAA Paper 98-3107, Jan. 1998.

[6] Romine, G. L., "Nozzle Flow Separation," *AIAA Journal*, Vol. 36, No. 9, 1998, pp. 1618–1625. doi:10.2514/2.588

[7] Papamoschou, D., and Zill, A., "Fundamental Investigation of Supersonic Nozzle Flow Separation," AIAA Paper 2004-1111, Jan. 2004.

[8] Xiao, Q., Tsai, H. M., and Papamoschou, D., "Numerical Investigation of Supersonic Nozzle Flow Separation," *AIAA Journal*, Vol. 45, No. 3, 2007, pp. 532–541. doi:10.2514/1.20073

[9] Carlson, J. R., "A Nozzle Internal Performance Prediction Method," NASA Technical Paper 3221, 1992.

[10] Xiao, Q., Tsai, H. M., and Liu, F., "Computation of Turbulent Separated Nozzle Flow by a Lag Model," *Journal of Propulsion and Power*, Vol. 21, No. 2, 2005, pp. 368–371. doi:10.2514/1.11446

[11] Sarkar, S., Erlebacher, G., Hussaini, M. Y., and Kreiss, H. O., "The Analysis and Modeling of Dilatational Terms in Compressible Turbulence," Institute for Computer Applications in Science and Engineering Technical Rept. 89-1789, 1989.

[12] Zeman, O., "Dilatation Dissipation: The Concept and Application in Modeling Compressible Mixing Layers," *Physics of Fluids A*, Vol. 2, 1990, pp. 178–188. doi:10.1063/1.857767

[13] Huang, P. G., Bradshaw, P., and Coakley, T. J., "Turbulence Model for Compressible Boundary Layers," *AIAA Journal*, Vol. 32, No. 4, 1994, pp. 735–740. doi:10.2514/3.12046

[14] Thies, A. T., and Tam, C. K. W., "Computation of Turbulent Axisymmetric and Nonaxisymmetric Jet Flows Using the k–ε Model," *AIAA Journal*, Vol. 34, No. 2, 1996, pp. 309–316. doi:10.2514/3.13065

[15] Tandra, D. S., Kaliazine, A., Cormack, D. E., and Tran, H. N., "Numerical Simulation of Supersonic Jet Flow using a Modified k–ε Model, *International Journal of Computational Fluid Dynamics*, Vol. 20, No. 1, 2006, pp. 19–27. doi:10.1080/10618560600587204

[16] Chenault, C. F., and Beran, P., "Numerical Investigation of Supersonic Injection Using a Reynolds-Stress Turbulence Model," *AIAA Journal*, Vol. 37, No. 10, 1999, pp. 1257–1269. doi:10.2514/2.594

[17] Zhang, H., So, R., Gatski, T., and Speziale, C., "A Near-Wall Second-Order Closure for Compressible Turbulent Flows," *Near-Wall Turbulent Flows*, edited by R. So, C. Speziale, and B. Launder, Elsevier, New York, 1993, pp. 209–218.

[18] Dembowski, M. A., and Georgiadis, N. J., "An Evaluation of Parameters Influencing Jet Mixing using the WIND Navier–Stokes Codes," NASA TM-2002-211727, 2002.

[19] Georgiadis, N. J., and Papamoschou, D., "Computational Investigation of High-Speed Dual-Stream Jets," AIAA Paper 2003-3311, June 2003.

[20] Menter, F. R., "Ten Years of Industrial Experience with the SST Turbulence Model," *Proceedings of the 4th International Symposium on Turbulence, Heat, and Mass Transfer*, International Centre for Heat and Mass Transfer, Ankara, Turkey, Oct. 2003, pp. 625–632.

[21] Spalart, P., and Allmaras, S., "A One-Equation Turbulence Model for Aerodynamic Flows," AIAA Paper 92-0439, Jan. 1992.

[22] Shih, T.-H., Liou, W. W., Shabbir, A., Yang, Z., and Zhu, J., "A New k–ε Eddy-Viscosity Model for High Reynolds Number Turbulent Flows-Model Development and Validation," *Computers & Fluids*, Vol. 24, No. 3, 1995, pp. 227–238. doi:10.1016/0045-7930(94)00032-T

[23] Wilcox, D. C., *Turbulence Modeling for CFD*, 1st ed., DCW Industries, Inc., La Canada, CA, 1993.

[24] Launder, B. E., Reece, G. J., and Rodi, W., "Progress in the Development of a Reynolds-Stress Turbulence Closure," *Journal of Fluid Mechanics*, Vol. 68, No. 3, 1975, pp. 537–566. doi:10.1017/S0022112075001814

K. Frendi
Associate Editor